#### **UCL**

# **Abstract**

**MAPS** 

MSci

#### Manganese Ferroelectric Instabilities in Perovskites and Porphyrins

by Oisin MORIARTY

This report presents a computational investigation of the structural and electronic properties of two distinct material classes that exhibit polar behaviour through metal centre displacement. The first system is a columnar perovskite that takes the form of NaY MnMnTi<sub>4</sub>O<sub>12</sub>. In this system, ferroelectricity originates from the interplay between partial A-site cation ordering and a ferroelectric instability associated with the pseudo Jahn Teller activity of square planar  $\mathrm{Mn^{2^+}}$  ions. Density functional theory calculations reveal that, in nearly all cation ordering configurations, the  $\mathrm{Mn^{2^+}}$  ions adopt an out-of-plane arrangement with an energetic advantage of approximately 0.11 eV compared to a square planar position. The redistribution of the d orbital energies, and in particular the marked lowering of the  $d_{xy}$  orbital, shares significant similarity with observations in  $\mathrm{Ca_{2-x}MnTi_2O_6}$ , suggesting that a similar underlying mechanism may govern the polar instability in both perovskite systems.

The second system comprises organic manganese compounds, including manganese porphyrins and phthalocyanines. In these molecular systems, forcing the Mn centre out of its ligand plane induces a clear transition from an intermediate spin state to a high spin state that is accompanied by a pronounced reorganisation of the d orbital occupancy. Although the high spin state is not energetically favoured in the organic molecules, the electronic response shows notable parallels with the behaviour seen in the Ca-based perovskite system. Possible improvements to the computational approach, such as the adoption of advanced functionals and the use of linear scaling techniques to model larger cell sizes, are also discussed. This work establishes a foundation for future studies aimed at designing multifunctional materials with controlled cation ordering, metal displacement, and spin state transitions.

# **Contents**

Al	ostrac	ct		i
1	Intr	oductio	on	1
		1.0.1	Ferroelectricity and Properties of Ferroelectric Materials	1
		1.0.2	An Investigation of Manganese Ferroelectric Instabilities	1
2	Bac	kgroun	d	5
	2.1	Novel	ferroelectric mechanisms	5
	2.2	Invest	rigating Ferroelectric Behaviour using Computational Models	7
		2.2.1	Density Functional Theory	7
		2.2.2	Self-Consistency and The Electronic Ground State	8
		2.2.3	Ionic Relaxation and Structure Optimization	8
		2.2.4	Post-Processing and Electronic Structure Analysis	8
		2.2.5	CONQUEST Implementation	9
3	Col	umnar	(NaY)MnMnTi4O12	11
	3.1	(NaY	)MnMnTi4O12 Background	11
		3.1.1	Method and Approach	11
		3.1.2	Cation Orderings	12
		3.1.3	Energy landscape	14
4	Por	hyrin	System	19
	4.1	Motiv	ration for presence of mechanism	19
		4.1.1	Method and Approach	19
		4.1.2	Energetics and Spin	20
		4.1.3	Variations of Molecule and Packing Arrangements	23
		4.1.4	Mn Displacement in Plane: Forced Symmetry Breaking	25
	4.2	Issues	Modelling High Spin Mn with DFT and Potential Solutions	27
		4.2.1	Ionic Relaxations	27
		4.2.2	Potential Solutions	27
5	Con	clusior	1	29

#### 1. Introduction

## 1.0.1 Ferroelectricity and Properties of Ferroelectric Materials

Ferroelectricity, the property of certain materials to maintain a spontaneous electric polarisation that can be reversed by the application of an external electric field. Since its discovery in Rochelle salt in 1921, and subsequently in barium titanate (BaTiO<sub>3</sub>) in the 1940s, ferroelectric materials have become essential components in numerous technological applications [1, 2].

Perovskite oxides, with their versatile ABO<sub>3</sub> structure constitute a major class of ferroelectric materials. The adaptability of the perovskite framework, capable of accommodating various elements in the periodic table at its A- and B-sites, gives rise to a wide range of properties. These include ferroelectricity, ferromagnetism, magnetoresistance, piezoelectricity, multiferroicity, and metal-insulator transitions [3, 4]. This structural versatility stems from the inherent instabilities of the cubic perovskite phase, which readily undergoes energy-lowering distortions that give rise to rich structural phase diagrams and diverse functional properties [5, 4].

The conventional understanding of ferroelectricity in perovskites has centred on two primary mechanisms. The first is the second-order Jahn-Teller effect driven by  $d^0$  transition metal cations (such as  $\mathrm{Ti}^{4+}$ ,  $\mathrm{Zr}^{4+}$ , or  $\mathrm{Nb}^{5+}$ ) at the B-site. The second is the stereochemical activity of lone-pair electrons in cations like  $\mathrm{Pb}^{2+}$  or  $\mathrm{Bi}^{3+}$  at the A-site [6, 7]. These classic mechanisms have provided the foundation for many of the most widely used ferroelectric materials, including  $\mathrm{BaTiO}_3$ ,  $\mathrm{PbTiO}_3$ , and  $\mathrm{Pb}(\mathrm{Zr},\mathrm{Ti})\mathrm{O}_3$  (PZT).

Recent advances in both theoretical understanding and experimental capabilities have shown that ferroelectric mechanisms are more complex than previously appreciated. Particularly intriguing is the recent discovery of "hybrid improper ferroelectricity," a mechanism where the coupling of two non-polar lattice modes can favour the activation of a third mode with a polar character [5]. This mechanism offers new pathways to multifunctionality by potentially allowing the coexistence of properties that have historically been difficult to combine, such as ferroelectricity and magnetism.

The significance of ferroelectric materials extends to numerous technological applications with substantial economic impact. The global market for ferroelectric materials and devices was valued at 73.4 billion USD in 2020 [8]. Ferroelectric capacitors are essential components in electronic circuits and energy storage devices. Ferroelectric random-access memory (FeRAM) offers faster write speeds and lower power consumption compared to many other memory technologies [9, 10]. The piezoelectric properties inherent to all ferroelectric materials have enabled the development of numerous sensors, actuators, and transducers. In photovoltaics, the bulk photovoltaic effect in certain ferroelectrics allows improved efficiency of solar cells [11, 10].

#### 1.0.2 An Investigation of Manganese Ferroelectric Instabilities

Within this context of expanding understanding and applications of ferroelectric materials, my research is motivated by the properties observed in the  $Ca_{2-x}Mn_xTi_2O_6$  perovskite system. This material demonstrates a departure from conventional ferroelectric mechanisms in perovskites, as explained by Benedek and Fennie [12] and presented in the following paragraphs.

2 1. Introduction

Traditionally, ferroelectricity and octahedral rotations appeared incompatible in perovskites. Typical ferroelectrics such as BaTiO<sub>3</sub> and PbTiO<sub>3</sub> do not exhibit octahedral rotations. Meanwhile, perovskites with octahedral rotations typically crystallise in nonpolar space groups. This incompatibility was puzzling because first-principles calculations showed that many materials with rotation-driven ground states actually possessed ferroelectric instabilities in their cubic phases.

Benedek and Fennie showed that it is not the octahedral rotations themselves that suppress ferroelectricity. Rather, it is the A-site cation displacements that accompany these rotations in structures like the common Pnma space group. These A-site displacements effectively compete with the polar mode, suppressing the ferroelectric instability. Their work suggested that materials with small tolerance factors and large octahedral rotations, but in structures where A-site displacements are symmetry-forbidden, could potentially exhibit novel ferroelectric behaviour.

The research presented in this report focuses on the recently discovered hybrid improper ferroelectric mechanism in the columnar perovskite (NaY)MnMnTi<sub>4</sub>O<sub>12</sub>. This material represents a novel realisation of hybrid improper ferroelectricity in columnar perovskites. Here, cation ordering on A-site columns, coupled with B-site octahedral tilts, results in a polar phase. The structure of (NaY)MnMnTi<sub>4</sub>O<sub>12</sub> is notable for hosting Mn<sup>2+</sup> ions in two distinct environments: tetrahedral coordination (Mn1) and pseudo-square planar coordination (Mn2). The latter Mn<sup>2+</sup> site exhibits a significant off-centering displacement similar to that observed in Ca<sub>2-x</sub>Mn<sub>x</sub>Ti<sub>2</sub>O<sub>6</sub>. This displacement appears to be influenced by the high-spin  $d^5$  electronic configuration of the Mn<sup>2+</sup> ions. The specific arrangement of electrons in the d orbitals and the resulting spin polarisation may play a crucial role in driving the ferroelectric behaviour.

In addition, my research extends beyond inorganic perovskites to examine similar manganese displacement mechanisms in organic systems, particularly manganese porphyrins. These molecular systems offer an opportunity to study the Mn displacement in relative isolation from the complex structural distortions present in perovskites. Detailed crystallographic studies of manganese porphyrins by Kirner et al. revealed that high-spin Mn<sup>2+</sup> exhibits significant thermal motion perpendicular to its square planar nitrogen coordination plane [14]. There is evidence suggesting positional disorder between two symmetry equivalent out-of-plane positions. This behaviour contrasts with other metal porphyrins where the central ion remains more rigidly centred. Further evidence for manganese's unique coordination behaviour comes from studies of metal phthalocyanines by Jiang et al. [15]. Quantum chemical analysis revealed that Mn-N interactions in similar square planar environments show distinct "shared interaction features" and strong metal-ligand bonding when compared to other first-row transition metals.

My research used density functional theory (DFT) calculations to investigate the electronic and structural properties of both systems. DFT provides a powerful framework for examining the quantum mechanical interactions that govern the behaviour of electrons in these materials, supporting deeper understanding of the relationship between electronic structure, spin polarisation, and structural distortions. I used the CONQUEST code, which offers both conventional cubic-scaling and linear-scaling DFT approaches, allowing for efficient simulations of large systems. Through these computational investigations, I aimed to identify common principles underlying the displacement behaviour of Mn ions across different material classes.

My specific areas for investigation were as follows. For  $(NaY)MnMnTi_4O_{12}$ , I aimed to analyse the polar ferroelectric phase to understand the effects of NaY cation ordering as well as to investigate spin polarisations to understand magnetic stacking

configurations. A key focus was on understanding the energetics of the ferroelectric transition, specifically with respect to the d-orbital occupation of Mn. In the case of the Porphyrin system, I aimed to investigate the energetics of Mn out-of-plane displacement to understand why it deviates from planarity as well as examining the spin polarisation of Mn and understanding the effects of crystallographic packing on the Mn displacement. Finally, I explored potential similarities with the improper ferroelectricity observed in the NaY perovskite system. Through this dual approach, I aimed to establish whether these seemingly different materials share common underlying mechanisms related to the Mn displacement phenomenon.

# 2. Background

The following section provides background on the novel ferroelectric mechanism discovered in the  $Ca_{2-x}Mn_xTi_2O_6$  perovskite and introduces the computational tools used throughout this project.

## 2.1 Novel ferroelectric mechanisms

Local polar displacements exist above the Curie temperature ( $T_c$ ), and only their ordering is temperature dependent. This unique feature has the potential to reduce the impact of depolarisation fields that typically suppress ferroelectricity in ultrathin films. Such pre-existing displacements motivate the exploration of novel ferroelectric mechanisms, such as that observed in the perovskite compound  $Ca_{2-x}Mn_xTi_2O_6$  [13].

The ferroelectric behaviour observed in  $Ca_{2-x}Mn_xTi_2O_6$  perovskites presents a novel mechanism for ferroelectricity that differs significantly from conventional ferroelectric materials [13]. The fundamental mechanism, illustrated in Figure 2.1, arises from the unique orbital physics of  $Mn^{2+}$  ions in coplanar coordination environments [13].

In this system, when  $Mn^{2+}$  occupies a coplanar site coordinated by four oxygen atoms, the crystal field creates a specific splitting of the d orbitals. Notably, the  $z^2$  orbital is energetically stabilised while the xy orbital is destabilised in this configuration. When the  $Mn^{2+}$  ion displaces out of the coordination plane, a significant reorganisation of orbital energies occurs. This displacement lowers the energy of the xy orbital, although it simultaneously raises the energies of the  $z^2$  and  $yz \pm izx$  orbitals. Crucially, the net energy balance favours the displaced configuration [13].

The mechanism becomes particularly evident when comparing  $Mn^{2+}$  to  $Fe^{2+}$ , which occupies the same site in the analogous  $CaFeTi_2O_6$  compound. Despite their similar ionic radii,  $Fe^{2+}$  remains in the coplanar position while  $Mn^{2+}$  displaces out of plane. This difference stems from the electronic configuration;  $Fe^{2+}$  has an additional electron in the  $z^2$  orbital compared to  $Mn^{2+}$ , significantly increasing the energetic penalty for displacement because moving out of plane would further destabilise the already doubly occupied  $z^2$  orbital [13].

What makes this system particularly interesting is the nature of the ferroelectric transition. Above  $T_c$ , the  $\mathrm{Mn}^{2+}$  ions are already displaced from the coplanar position, but these displacements occur in random directions along the c axis. When the temperature drops below  $T_c$ , these displacements become ordered, with all  $\mathrm{Mn}^{2+}$  ions displacing in the same direction. This ordering creates a net polarisation throughout the material. Additionally, this ordering induces displacements in the  $\mathrm{Ti}^{4+}$  ions, which further contributes to the overall polarisation [13].

This order-disorder type transition differs fundamentally from the displacive transitions observed in conventional ferroelectrics like BaTiO<sub>3</sub>, where ions move from centrosymmetric to polar positions at the transition temperature [13].

6 2. Background

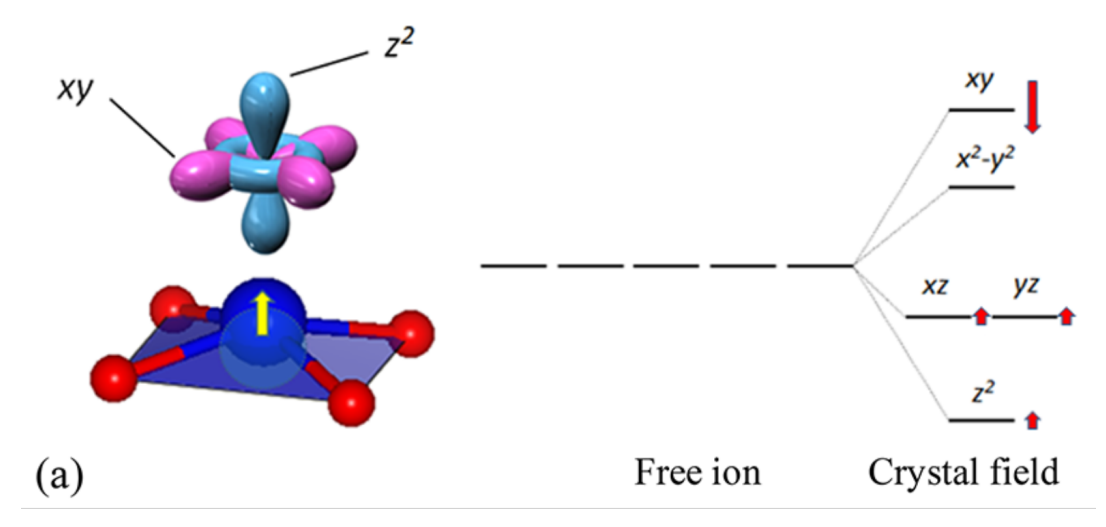


FIGURE 2.1: The figure illustrates the orbital behavior of Mn in MnO structures, showing how the d-orbitals (xy and z²) arrange spatially and undergo energy splitting when transitioning from free ion state to crystal field environment. The diagram depicts the Mn displacement from the plane formed by four oxygen anions, with red arrows indicating energy changes corresponding to this movement. The length of these arrows represents the magnitude of energy change during displacement. The orbital diagram shows the distribution of electron spins (indicated by blue arrows) and explains how the specific orbital occupancy affects the positioning of the metal ion relative to the oxygen plane. This representation is based on density functional theory calculations detailed in supplementary materials. Figure adapted from [13]

# 2.2 Investigating Ferroelectric Behaviour using Computational Models

Fundamentally, this project involved applying computational models to real materials to explore the mechanisms underlying ferroelectric observed behaviour, particularly those involving the intriguing role of high-spin manganese ions. Various methods exist for atomistic modelling, each with its own strengths and limitations regarding accuracy, computational cost, and applicability to the specific complexities of a given system.

Classical approaches, relying on empirical force fields parametrised against experimental data or high-level calculations, offer significant computational efficiency, enabling the simulation of large systems and long timescales. However, these force fields often struggle to accurately describe the intricate electronic rearrangements and quantum mechanical effects that are crucial for understanding ferroelectricity, especially phenomena driven by transition metal d-electrons like those in manganese. These effects include subtle changes in bonding, charge transfer, and the influence of spin states, which are central to our investigation of Mn<sup>2+</sup> displacement and its impact on ferroelectric polarization.

While semi-empirical methods(Hartree-Fock theory and post-Hartree-Fock methods) offer improved accuracy by explicitly treating some aspects of electronic structure, they typically incur substantial computational costs, limiting their applicability to the relatively large unit cells and complex chemical environments often encountered in perovskite and porphyrin systems. Given the need to accurately capture the electronic origins of ferroelectricity, including the role of Mn's d-electron configuration and spin polarization, while remaining computationally feasible for the systems of interest, Density Functional Theory (DFT) emerges as the most appropriate method.

DFT balances computational efficiency with a detailed treatment of electronic exchange and correlation effects [16, 17], thereby providing a robust framework that connects computational predictions directly to experimentally observable properties relevant to ferroelectricity and magnetism.

### 2.2.1 Density Functional Theory

Density Functional Theory is founded on the Hohenberg-Kohn theorems [16], which establish that the ground-state energy of a many-electron system is uniquely determined by its electron density,  $\rho(\mathbf{r})$ , rather than by the complex many-body wavefunction,  $\Psi$ . This fundamental insight allows bypassing the exponential complexity of many-body wavefunctions by working directly with the electron density. The interacting electron system is mapped onto a system of non-interacting Kohn-Sham electrons [17]. In this formulation, the central operator is the Kohn-Sham Hamiltonian,

$$\hat{H}_{KS} = -rac{1}{2}
abla^2 + V_{\mathrm{ext}} + V_H + V_{\mathrm{XC}},$$

where  $V_{\text{ext}}$  is the external potential from the nuclei,  $V_H$  is the classical electrostatic (Hartree) potential, and  $V_{\text{XC}}$  is the exchange-correlation potential that accounts for the remaining quantum mechanical interactions. This Hamiltonian operates on the Kohn-Sham orbitals,  $\psi_k(\mathbf{r})$ , yielding the eigenvalues  $E_k$  according to

$$\hat{H}_{KS}\psi_k(\mathbf{r})=E_k\psi_k(\mathbf{r}).$$

8 2. Background

The electron density is subsequently constructed from these orbitals,

$$\rho(\mathbf{r}) = \sum_{k} |\psi_k(\mathbf{r})|^2.$$

The total energy of the system is written as

$$E_{\text{tot}} = E_{\text{KE}} + E_{\text{eI}} + E_{H} + E_{\text{XC}} + E_{\text{II}},$$

where the exchange-correlation energy,  $E_{XC}$ , is typically approximated using methods such as the Local Density Approximation (LDA) or the Generalized Gradient Approximation (GGA) [17].

#### 2.2.2 Self-Consistency and The Electronic Ground State

The solution of the Kohn-Sham equations is inherently self-consistent. The process begins with an initial guess for the electron density, which determines the effective potential in the Kohn-Sham Hamiltonian. Solving the resulting eigenvalue problem yields a new set of Kohn-Sham orbitals and an updated electron density. This iterative cycle continues until the changes in total energy or electron density between successive iterations fall below a predetermined threshold, confirming convergence [25]. The need for self-consistency arises because the Hartree and exchange-correlation potentials depend on the electron density, creating a feedback loop that must be resolved through iteration.

#### 2.2.3 Ionic Relaxation and Structure Optimization

After electronic self-consistency is achieved, the next step is to optimize the atomic structure by relaxing the ionic positions. The forces acting on the atoms are obtained using the Hellmann-Feynman theorem,

$$\mathbf{F}_I = -\frac{\partial E_{\text{tot}}}{\partial \mathbf{R}_I}.$$

These forces drive the adjustment of atomic positions via minimization algorithms such as the conjugate gradient or BFGS methods. The goal is to reduce the forces on all atoms to negligible levels, thereby locating the equilibrium positions. This step is especially critical for ferroelectric materials, where subtle displacements (for example, the off-center movement of Mn<sup>2+</sup> ions) are key to the material's properties [?].

#### 2.2.4 Post-Processing and Electronic Structure Analysis

Once both electronic and ionic relaxations are complete, further analysis of the electronic structure provides deeper insight into the material properties. The Projected Density of States (PDOS) method, for example, decomposes the total density of states by projecting it onto the atomic orbitals. In systems such as Mn<sup>2+</sup> with a high-spin d<sup>5</sup> configuration, PDOS analysis reveals details of orbital splitting and occupation:

PDOS<sub>$$\alpha$$</sub>(E) =  $\sum_{n} |\langle \phi_{\alpha} | \psi_{n} \rangle|^{2} \delta(E - E_{n})$ ,

where  $\phi_{\alpha}$  represents the basis of atomic orbitals and  $\psi_n$  are the Kohn-Sham eigenstates [21]. Additionally, Mulliken population analysis partitions the electron density among the atoms by using the density matrix  $P_{\mu\nu}$  and the overlap matrix  $S_{\mu\nu}$  to

yield quantitative information on charge distribution and bonding:

$$q_A = \sum_{\mu \in A} \sum_{\nu} P_{\mu\nu} S_{\mu\nu}.$$

This analysis is invaluable for examining the bonding interactions between Mn<sup>2+</sup> and its coordinating atoms, thereby clarifying the electronic origin of ferroelectricity [18].

## 2.2.5 CONQUEST Implementation

For this work, I used the CONQUEST implementation of Density Functional Theory. CONQUEST is a highly efficient, parallelized DFT code well-suited for studying the complex structural and electronic properties of the systems of interest. Its parallel scaling allows for efficient utilization of high-performance computing resources, which is essential for handling the computational demands of DFT calculations, especially when performing extensive structural relaxations to understand the energy landscape associated with Mn ion displacements.

While CONQUEST provides a powerful framework, the accuracy of DFT calculations, in general, depends on the chosen exchange-correlation functional. As discussed in the previous section on DFT Theory, approximations like LDA and GGA have known limitations, particularly in accurately describing strongly correlated systems, which can be relevant to transition metal oxides with localized d-electrons, such as those involving Mn. Therefore, careful selection and validation of the functional are crucial. Furthermore, the choice of basis set can influence the accuracy and convergence of the calculations, necessitating convergence tests.

In summary, CONQUEST offers a computationally efficient and parallelize-able environment for DFT investigations. However, it is important to be mindful of the inherent limitations of DFT and the specific choices made within CONQUEST (functional, basis set) to ensure the reliability and accuracy of results.

The CONQUEST code implements DFT using a density matrix formalism in which the electron density is expressed in terms of localized support functions,  $\phi_{i\alpha}(\mathbf{r})$ , as follows:

$$\rho(\mathbf{r},\mathbf{r}') = \sum_{i\alpha,j\beta} \phi_{i\alpha}(\mathbf{r}) K_{i\alpha,j\beta} \phi_{j\beta}(\mathbf{r}'),$$

with  $K_{i\alpha,j\beta}$  being the density matrix expressed in this basis [22]. The density matrix must satisfy three conditions: proper normalization to ensure the correct electron count, idempotency (i.e.,  $K^2 = K$ ), and energy minimization. The McWeeny transformation is commonly applied to enforce idempotency:

$$K_{\text{new}} = 3K_{\text{out}}^2 - 2K_{\text{out}}^3.$$

Convergence is further accelerated by employing Direct Inversion in the Iterative Subspace (DIIS), which optimizes the density matrix by minimizing the residual error using previous iterations [23]. An additional challenge known as charge sloshing especially prevalent in metallic systems and at surfaces is managed through the use of Kerker preconditioning:

$$f(q) = \frac{q^2}{q^2 + q_0^2},$$

which dampens long-wavelength fluctuations in the charge density by properly tuning the parameter  $q_0$  [26].

### 3. Columnar (NaY)MnMnTi4O12

The following section looks at the newly discovered (NaY)MnMnTi<sub>4</sub>O<sub>12</sub> with a particular focus on the manganese instability in its polar phase.

# 3.1 (NaY)MnMnTi4O12 Background

The columnar perovskite (NaY)MnMnTi<sub>4</sub>O<sub>12</sub> (shown in Figure 3.1) provides a valuable comparative system to further explore the ferroelectric displacement mechanisms identified in  $Ca_{2-x}Mn_xTi_2O_6$ .

This compound was synthesized using high-pressure methods at 6 GPa from stoichiometric mixtures of MnO,  $Na_2TiO_3$ ,  $Y_2O_3$ , and  $TiO_2$ . Significantly, the annealing temperature during synthesis determines the resulting crystal structure, with low-temperature annealing (LTA) at 1550 K producing a polar phase and high-temperature annealing (HTA) at 1750 K yielding a centrosymmetric phase.

The crystal structure of (NaY)MnMnTi $_4$ O $_{12}$  features a columnar arrangement where Na $^+$  and Y $^{3+}$  cations occupy A-site columns along the c-axis, surrounded by a framework of corner-shared TiO $_6$  octahedra. Mn $^{2+}$  ions are distributed across both square-planar (A') and tetrahedral (A'') coordination environments. The octahedral tilting pattern (a $^+$ a $^+$ c $^-$ ) intrinsically creates oppositely displaced A-site columns.

The ferroelectric instability in this material appears to arise through two complementary mechanisms. First, a hybrid improper ferroelectric mechanism occurs when partial ordering of Na<sup>+</sup> and Y<sup>3+</sup> cations between the oppositely displaced columns breaks inversion symmetry. The second mechanism involves a proper ferroelectric instability associated with Mn<sup>2+</sup> ions at the square-planar sites, which exhibit pseudo-Jahn-Teller (pJT) activity. This may be similar to the Mn<sup>2+</sup> displacement observed in Ca<sub>2-x</sub>Mn<sub>x</sub>Ti<sub>2</sub>O<sub>6</sub>, where orbital energy redistribution could drive the displacement of Mn<sup>2+</sup> from its ideal position. Examining whether the d<sub>xy</sub> orbital energy is lowered while the d<sub>z²</sub> orbital energy increases when Mn<sup>2+</sup> moves out of the plane, as observed in Ca<sub>2-x</sub>Mn<sub>x</sub>Ti<sub>2</sub>O<sub>6</sub>, could demonstrate whether similar electronic considerations are at play in both materials.

In the following sections, the role of cation ordering on the displacement of the  $Mn^{2+}$  ions is investigated. The energetics of the  $Mn^{2+}$  transition are also explored and compared to those present in the  $Ca_{2-x}Mn_xTi_2O_6$  study.

## 3.1.1 Method and Approach

To further investigate the interplay between columnar A-site cation ordering and Mn displacement in the polar phase of (NaY)MnMnTi $_4$ O $_{12}$ , a series of computational experiments using CONQUEST DFT were conducted. Different arrangements of Na $^+$  and Y $^{3+}$  were systematically explored to understand their effect on the displacement behaviour of square-planar Mn $^{2+}$  ions and their corresponding electronic and energetic properties.

As shown in Figure 3.2, three distinct columnar ordering patterns were examined: (i) fully ordered columns, where each column contains exclusively either  $Na^+$  or  $Y^{3+}$  cations; (ii) out-of-phase ordering, where  $Na^+$  and  $Y^{3+}$  cations alternate within columns but with an out-of-phase relationship between adjacent columns; and (iii) in-phase ordering, where  $Na^+$  and  $Y^{3+}$  cations alternate within columns and maintain an in-phase relationship between adjacent columns.

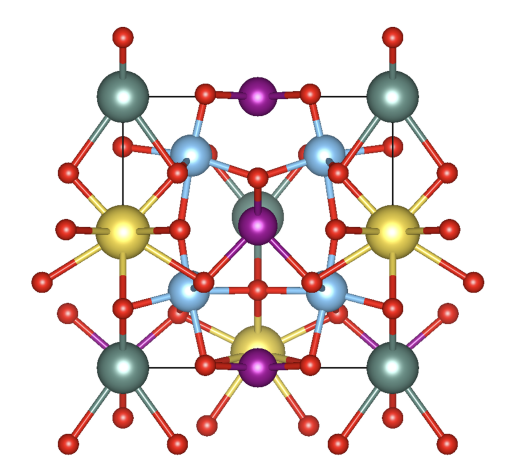


FIGURE 3.1: Crystal structure of the quadruple perovskite (NaY)MnMnTi4O12 showing the complex arrangement of cations. The structure features Na (yellow) and Y (green) at the A-sites, Mn (purple) occupying both square-planar coordinated A'-sites and tetrahedral A''-sites, Ti (light blue) at the B-sites, and oxygen (red) forming the corner-sharing octahedral framework.

For each ordering pattern, the square-planar Mn<sup>2+</sup> ions were displaced in various configurations along the c-axis: both displaced upward, both downward, alternating upward and downward in different sequences, and in-plane positions. The computational approach involved a three-step procedure using the CONQUEST code: initial ionic relaxation with fixed cell parameters, followed by full cell relaxation, and finally a static calculation to analyse the electronic structure. In order to measure the displacement of the Mn<sup>2+</sup> ions from their square planar site a Python script to fit a plane to the four oxygen atoms. The displacement of the ion was then defined as the perpendicular distance from the plane.

### 3.1.2 Cation Orderings

The results demonstrated a strong preference for the Mn² ions to sit out-of-plane in almost all configurations. This confirmed the ferroelectric nature of the perovskite that had been observed experimentally. One notable counter example was in the case of the in-phase columnar ordering, calculations showed that when Mn ions were initially placed in an alternating upward-downward configuration, they tended to move back toward the square-planar positions during relaxation. This can be seen in Figure 3.3. This behaviour was not observed at all in the fully ordered or out-of-phase arrangements, suggesting that the specific arrangement of Na and Y³ cations directly influences the stability of Mn displacements.

The relationship between A-site cation ordering and Mn ion displacement appears more nuanced than initially expected. As shown in the figure, in the in-phase ordering, the behaviour varies depending on the specific configuration. While the +- configuration maintains significant out-of-plane displacement, the -+ configuration shows Mn ions returning almost completely to their square-planar positions. This suggests that the electrostatic interactions between A-site cations and Mn ions are more complex than a simple uniform distribution effect and it is not just nearest neighbour interactions with the ions that matter but also Mn-Mn interactions.

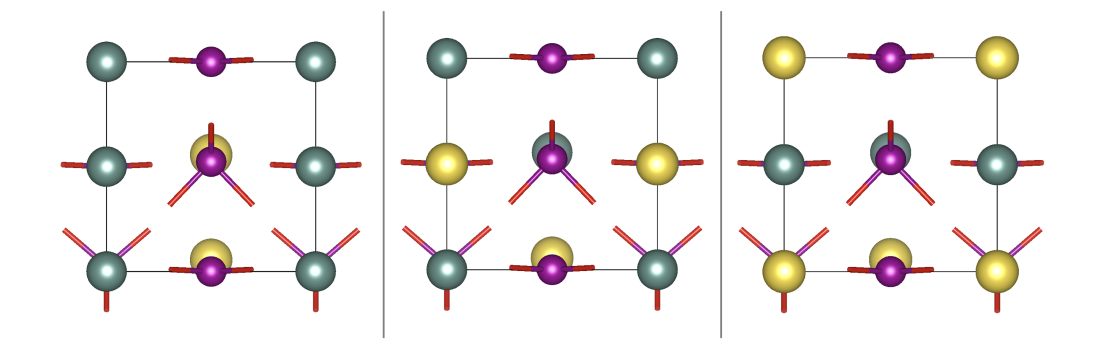


FIGURE 3.2: Structural models of different columnar ordering patterns in (NaY)MnMnTiO. Left panel shows fully ordered columns where each column contains exclusively either Na (yellow) or Y³ (green). Center panel displays out-of-phase ordering where Na and Y³ cations alternate within columns with out-of-phase relationship between columns. Right panel shows in-phase ordering with alternating Na/Y³ maintaining the same phase across columns. Purple spheres represent Mn² ions in both square-planar and tetrahedral coordination environments.

TABLE 3.1: Combined Mn displacements in Å, planarity, and coordination plane angles for (NaY)MnMnTi $_4$ O $_{12}$ . Displacements were converted from bohr (1 bohr = 0.529177 Å). Results are grouped into three ordering patterns: In-phase Ordering, Out-of-phase Ordering, and Fully Ordered. The configuration symbols (++, +-, -+, -) denote the displacement directions. Mn7 and Mn8 are labels given to Manganese atoms, defined on alternating planes with oppossing spin polarisations.

Displacement	Mn7 Disp. (Å)	Mn8 Disp. (Å)	Mn7 Planarity	Mn8 Planarity	Angle Z Mn7 (rad)	Angle Z Mn8 (rad)		
In-phase Ordering								
++	0.420450	0.400 622	0.000 180	0.000294	0.010753	0.015 951		
+-	0.400210	0.381 886	0.000144	0.000152	0.009659	0.002805		
-+	0.006823	0.012 137	0.000244	0.000 006	0.021 700	0.013 800		
	0.403279	0.388 966	0.000792	0.000313	0.005227	0.064071		
			Out-of-phase C	Ordering				
++	0.468 051	0.292771	0.000075	0.000 003	0.042 281	0.054621		
+-	0.448 163	0.263 440	0.000212	0.000168	0.057 537	0.033 125		
-+	0.462561	0.279604	0.000016	0.000044	0.035 638	0.053 939		
	7.378 535	0.458537	0.000634	0.000047	0.040740	0.025248		
			Fully Orde	ered				
++	0.474734	0.477 283	0.000403	0.000307	0.094 186	0.012307		
+-	0.460 996	0.461 162	0.000 133	0.000407	0.031 232	0.029865		
-+	0.462361	0.462852	0.000022	0.000253	0.084 556	0.019860		
	0.463744	0.464687	0.000367	0.000340	0.090 089	0.006 114		

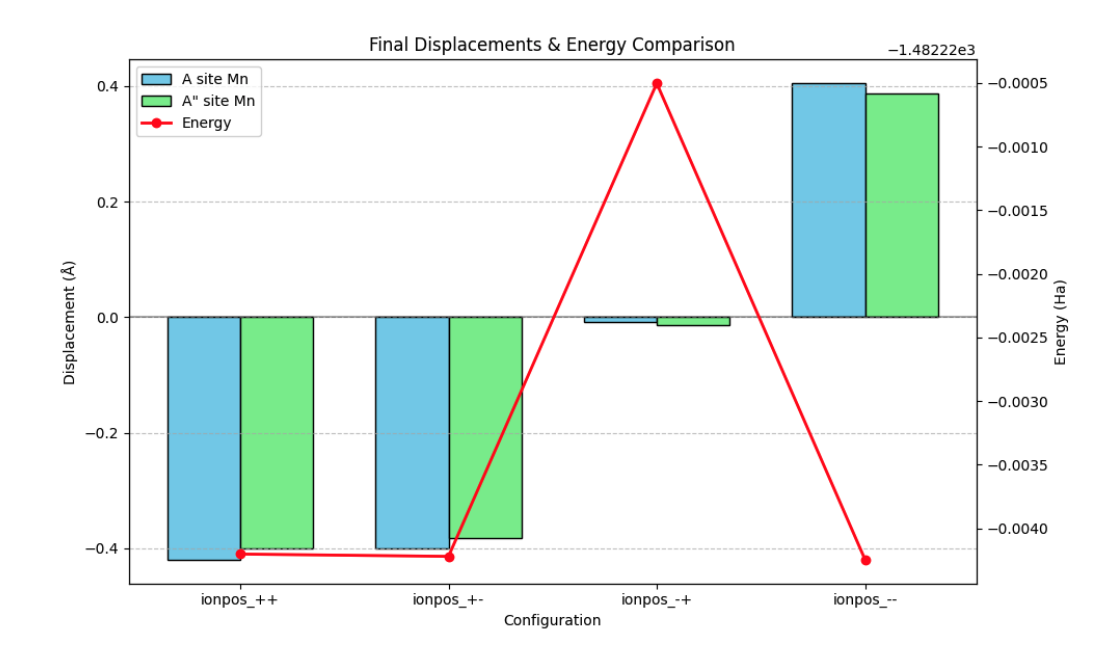


FIGURE 3.3: Final displacements of the two square-planar Mn² sites (A site and A site) in (NaY)MnMnTiO for four different initial displacement configurations: ++, +-, -+, and -. where "+" denotes an upward displacement and "-" denotes a downward displacement. The bar chart (left axis) indicates the magnitude and direction (upward or downward) of Mn² off-centre distortion from its square-planar position, while the red line (right axis) shows the corresponding Harris–Foulkes energies obtained from DFT calculations.

In contrast, both the fully ordered and out-of-phase configurations consistently promote off-centre Mn displacements across all tested configurations. The asymmetric electrostatic environments created in these ordering patterns appear to stabilize the ferroelectric distortions, though with varying magnitudes depending on the specific arrangement. This configuration-dependent behaviour highlights the importance of not just the overall ordering pattern but also the specific positions of the Manganese atoms in relation to these ions.

The magnetic ordering of Mn ions displays a type-C antiferromagnetic structure, as shown in Table 3.4. The Mn7 and Mn8 atoms, situated on alternating ab planes along the c-axis, consistently exhibit opposite magnetic moments of approximately  $-4.7~\mu_B$  and  $+4.7~\mu_B$ , respectively. This antiparallel alignment persists across all ordering configurations, indicating that the antiferromagnetic coupling between planes is primarily determined by Mn–Mn exchange pathways rather than being influenced by A-site cation ordering. Within each ab plane, magnetic moments maintain a uniform direction, creating a robust magnetic structure that remains stable regardless of changes in the A-site arrangement.

#### 3.1.3 Energy landscape

The calculated Harris-Foulkes energies for different Na/Y ordering patterns and Mn displacement configurations are presented in Table 3.2. These results show the energetic stability of various structural arrangements in (NaY)MnMnTi $_4$ O $_{12}$ .

A striking observation was that for the in-phase ordering pattern, the -+ configuration (where one Mn is displaced upward and one downward) exhibits a notably

TABLE 3.2: Combined Harris-Foulkes Energies (Ha) for different Na/Y ordering patterns. The ordering type is indicated by the subheadings, and the configuration symbols (++, +-, -+, -) denote the initial displacement directions.

Displacement	Harris-Foulkes Energy (Ha)
In-phase Orderii	ng
++	-1482.224202
+-	-1482.224220
-+	-1482.220504
	-1482.224245
Out-of-phase Or	dering
++	-1482.224500
+-	-1482.223919
-+	-1482.224500
	-1482.224449
Fully Ordered	
++	-1482.247068
+-	-1482.247184
-+	-1482.247185
	-1482.247 190

higher energy compared to the other in-phase configurations. As shown in Figure 3.3, in this particular case, the Mn ions remained close to their square-planar positions rather than displacing significantly out-of-plane. This gave an estimate for the energy penalty for  $Mn^{2+}$  ions remaining in-plane at approximately 0.004 Ha (about 0.11 eV), representing the energetic barrier that must be overcome for the ions to return to their undistorted positions.

Furthermore, comparing the three different Na/Y ordering patterns showed that the fully ordered arrangement consistently yields the lowest energy states, with values approximately 0.023 Ha (0.63 eV) lower than both the in-phase and out-of-phase configurations. This significant energy difference indicates that the fully ordered columnar arrangement, where each column contains exclusively either Na $^+$  or Y $^{3+}$  cations, provided the most stable electrostatic environment for the system.

To explore the electronic origins of these energy differences and to compare the  $\mathrm{Mn^{2+}}$  displacement mechanism in (NaY)MnMnTi<sub>4</sub>O<sub>12</sub> with that observed which was observed in  $\mathrm{Ca_{2-x}Mn_xTi_2O_6}$ , I analysed the projected density of states (pDOS) for the Mn d-orbitals in two contrasting cases: the out-of-plane configuration (++) from the in-phase ordering and the in-plane configuration (-+) also from the in-phase ordering. As seen in Table 3.3, the occupations of the d-orbitals were consistent with those observed for Mn in  $\mathrm{Ca_{2-x}Mn_xTi_2O_6}$ , with roughly speaking one electron on each orbital. Two methods had been utilised to determine the oxidation states of the  $\mathrm{Mn^{2+}}$  ions, as illustrated in Table 3.4: a Mulliken analysis and an empirical approach. In the empirical approach the bond valence was defined as

$$bv = \exp\left(\frac{R_0 - R}{B}\right),\tag{3.1}$$

where R was the bond length (in Å), and  $R_0$  and B were empirical parameters. In the case of Mn–O bonds, they were reported as: [40]

$$R_0 = 1.765 \,\text{Å}$$
 and  $B = 0.37$ .

The bond valence for each nearest-neighbour was computed using Equation 3.1 and then to sum these values in order to obtain an estimate of the Mn valence. These results show the oxidation state of Mn being somewhere between +1 and +2. This is roughly inline with the Mn2+ picture found in  $Ca_{2-x}Mn_xTi_2O_6$ . Given the similar bonding environments this is to be expected.

TABLE 3.3: Comparison of orbital occupation between out-of-plane and in-plane Mn<sup>2+</sup> configurations.

2*Orbital	Out-of-plane (++) configuration			In-plane (-+) configuration		
	Spin-up	Spin-down	Net (↑-↓)	Spin-up	Spin-down	Net $(\uparrow -\downarrow)$
Total	5.1911	0.5662	4.6249	5.1543	0.5660	4.5883
$d_{z^2}$	0.8994	0.1286	0.7708	0.8581	0.1494	0.7087
$d_{xz}$	0.9840	0.0497	0.9343	0.9937	0.0428	0.9509
$d_{yz}$	0.9678	0.0525	0.9153	0.9541	0.0585	0.8956
$d_{x^2-y^2}$	0.9922	0.0647	0.9275	0.9940	0.0431	0.9510
$d_{xy}$	0.9906	0.0629	0.9278	0.9915	0.0751	0.9164
d total	4.8341	0.3584	4.4757	4.7914	0.3689	4.4225

Now that similarities in the bonding environment, oxidation and occupations have been established, the d-orbital energetics can be compared. As seen in Figure 3.4, there is a reduction in energy associated with the  $d_{xy}$  orbital and a very slight increase associated with the  $d_{z^2}$  orbital as the manganese moves from its in-plane to out-of-plane configuration. However, unlike the mechanism outlined by Li et al., the  $d_{xz}$  and  $d_{x^2-y^2}$  orbitals both see decreases in energy when moving out of plane, not increases. Furthermore, in the crystal field splitting, the  $d_{z^2}$  orbital sits slightly higher than it did in the mechanism outlined by Li et al. and seen in Figure 2.1.

The fully ordered Na/Y arrangement likely enhances this effect by creating a more asymmetric electrostatic environment that further stabilizes the  $\mathrm{Mn^{2+}}$  displacement, explaining its significantly lower energy compared to the other configurations. This interplay between cation ordering and Mn displacement demonstrates how the ferroelectric behaviour in (NaY)MnMnTi<sub>4</sub>O<sub>12</sub> emerges from a complex combination of structural and electronic factors. While there are clearly strong similarities between the manganese displacement in the (NaY)MnMnTi<sub>4</sub>O<sub>12</sub> and that outlined for  $\mathrm{Ca_{2-x}Mn_xTi_2O_6}$ , the differences in d-orbital energy distributions make it difficult to draw concrete conclusions about the presence of this mechanism in  $\mathrm{Ca_{2-x}Mn_xTi_2O_6}$ . In the following section, organic systems will be examined to gain a better understanding of this mechanism in a more isolated environment.

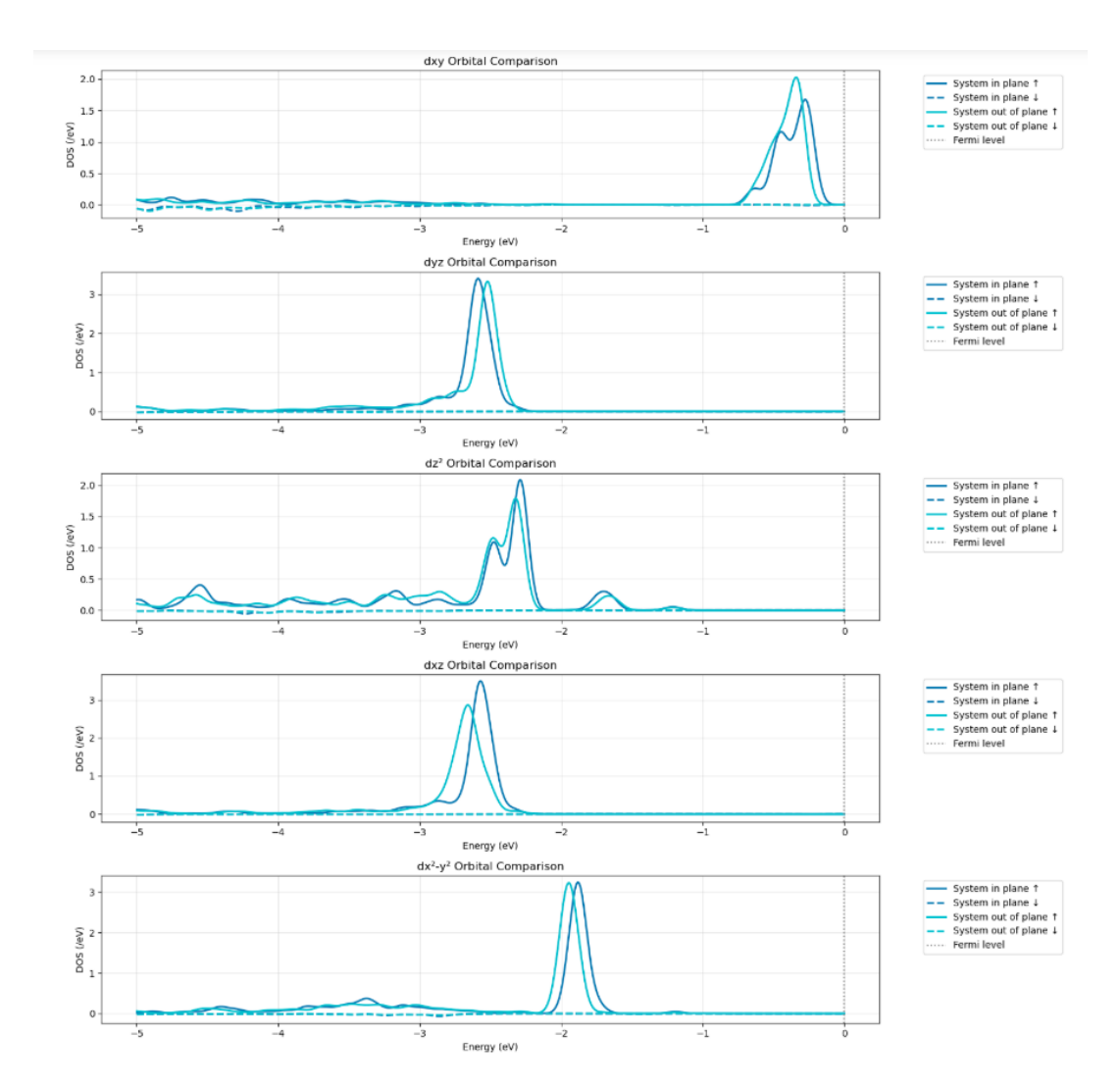


FIGURE 3.4: Density of states (DOS) comparison showing the dorbital energies for  $\mathrm{Mn^{2+}}$  (Mn8) in both in-plane and out-of-plane configurations. The plots display the spin-up resolved density for each of the five d-orbitals:  $\mathrm{d}_{xy}$  (top),  $\mathrm{d}_{yz}$  (second),  $\mathrm{d}_{z^2}$  (middle),  $\mathrm{d}_{xz}$  (fourth), and  $\mathrm{d}_{x^2-y^2}$  (bottom). Blue solid and dashed lines represent the in-plane configurations, while teal solid and dashed lines show the out-of-plane configurations. The  $\mathrm{d}_{xz}$  orbital shows the most significant energy reduction upon displacement from the plane, while  $\mathrm{d}_{yz}$  shows a slight increase in energy. Unlike the mechanism proposed by Li et al., the  $\mathrm{d}_{xz}$  and  $\mathrm{d}_{x^2-y^2}$  orbitals also show energy decreases rather than increases when  $\mathrm{Mn^{2+}}$  moves out of plane. Almost all spin density is in the spin-up channel, consistent with high-spin  $\mathrm{Mn^{2+}}$  (S = 5/2).

TABLE 3.4: A comparison of Mn7 and Mn8 Oxidation states, using Muliken analysis and an emperical results to estimate oxidation.

2*Displacement		Mn7			Mn8			
	Diff	Oxidation (Mulliken)	Oxidation (BV sum)	Diff	Oxidation (Mulliken)	Oxidation (BV sum)		
In-phase Ordering								
++	-4.681764	1.122 624	1.532 495	4.662352	1.105 070	1.651 567		
+-	-4.675904	1.129 145	1.563 167	4.658484	1.109 583	1.672 387		
-+	-4.665002	1.182 880	1.707 217	4.629 966	1.166414	1.837 405		
	-4.681070	1.124 910	1.541 754	4.660448	1.108 819	1.667 048		
Out-of-phase Ordering								
++	-4.694224	1.096 665	1.494 166	4.694333	1.096 460	1.661 284		
+	-4.695193	1.098 307	1.502 502	4.694784	1.098 561	1.669 537		
-+	-4.695025	1.098 107	1.492 155	4.695079	1.098 105	1.657 486		
	-4.695546	1.097 954	1.671 476	4.695541	1.097 949	1.502 829		
Fully Ordered								
++	-4.680212	1.091 945	1.473 210	4.680071	1.143 224	1.472 038		
+-	-4.678042	1.097 487	1.476 164	4.679316	1.150 597	1.477 455		
-+	-4.680713	1.093 061	1.476 748	4.682553	1.144084	1.477 184		
	-4.678666	1.146 443	1.473 546	4.679514	1.094 340	1.473 384		

# 4. Porphyrin System

Whilst (NaY)MnMnTi<sub>4</sub>O<sub>12</sub> provided an interesting comparison to the manganese displacement mechanism observed in  $Ca_{2-x}Mn_xTi_2O_6$ , the differences in the d-orbital energy shifts on manganese remained unclear. Therefore, to further explore this mechanism, manganese porphyrin compounds were investigated. They provided an isolated environment in which to study the mechanism, free from the interactions with surrounding cations present in (NaY)MnMnTi<sub>4</sub>O<sub>12</sub>. Furthermore, these compounds featured similar bonding environments, with manganese coordinated in a square-planar nitrogen geometry (although this was in contrast to the oxygen coordination observed in the perovskites). Finally, there was evidence that the manganese tended to adopt an out-of-plane position. The following pages present an exploration of this mechanism and examine whether it was present in a variety of different molecules.

# 4.1 Motivation for presence of mechanism

Kirner, Reed, and Scheidt's crystallographic study of manganese tetraphenylporphyrin (MnTPP) [14] provides compelling evidence that similar structural phenomena may exist in porphyrinoid systems. Their work reveals significant ambiguity regarding the position of the manganese atom relative to the porphyrin plane, with thermal parameters suggesting either substantial vibrational motion perpendicular to the plane or positional disorder with the metal distributed between two symmetry-equivalent out-of-plane positions. This parallel to the A'-site displacement mechanism in perovskites offers an opportunity to investigate similar electronic effects in a more accessible molecular system.

If the mechanism identified in the  $Ca_{2-x}Mn_xTi_2O_6$  perovskite is indeed present in our manganese porphyrin systems, we expect to observe several key indicators. First, we will look for specific changes in the electronic configuration and spin state of the manganese centre as it moves out of the porphyrin plane. The formal oxidation state and d-electron count of the manganese should remain constant, but the effective distribution of charge between the metal and ligand may shift. Particularly significant would be changes in the energetic ordering of d-orbitals, especially the dxy, dxz/dyz, and dz² orbitals, which Wallace et al. [3]identified as critical in determining the ground state electronic configuration of manganese phthalocyanines.

We will also investigate the energetics associated with the out-of-plane displacement of the manganese atom. If analogous to the perovskite mechanism, there should be a clear energy advantage to the Mn ion sitting out of plane.

#### 4.1.1 Method and Approach

To investigate the parallels between perovskite ferroelectrics and molecular systems such as MnTPP, the simplest case of manganese porphyrin (MnP), as shown in Figure 4.1, was utilised initially. An ionic relaxation with an initial spin polarisation of magnitude  $S=\frac{5}{2}$  on the Mn centre was performed. Subsequently, a series of static calculations on closely packed manganese porphyrin systems was carried out. In these static calculations, the electronic structure was determined without allowing

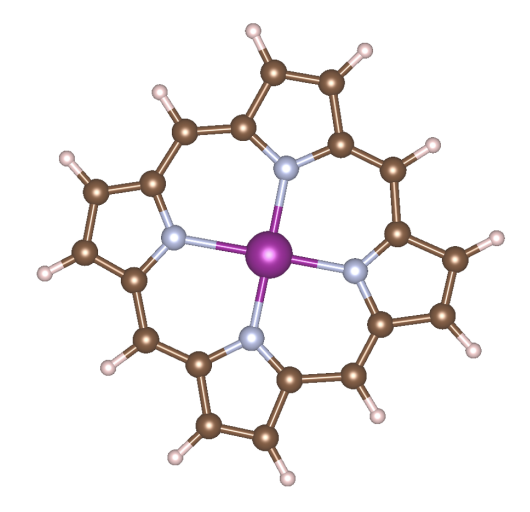


FIGURE 4.1: Manganese Porphyrin Molecule. Purple: Manganese, Blue: Nitrogen, Brown: Carbon, Pink: Hydrogen.

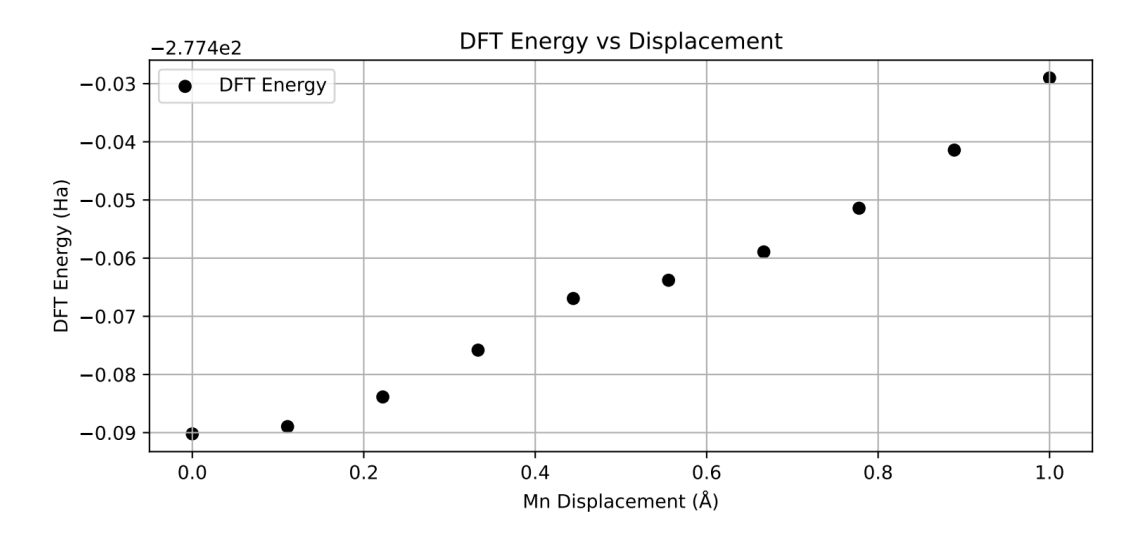


FIGURE 4.2: Enter Caption

atomic positions to relax, thereby enabling a systematic mapping of the potential energy surface for specific displacements of the manganese ion and further exploration of the associated effects.

For this investigation, several porphyrin configurations were examined using the method outlined above. These included stacked systems in which the nitrogen atoms were positioned directly above the manganese centres, as well as systems with direct stacking. For each configuration, a set of calculations was performed that varied the manganese displacement from the in-plane position to displacements of up to 1 Å. Furthermore, the role of the spin state in the metal displacement mechanism was investigated by testing distinct spin configurations for the manganese centre.

## 4.1.2 Energetics and Spin

An initial ionic relaxation of MnP showed that the manganese remained in-plane and the structure remained flat. Furthermore, a spin polarisation of magnitude S =

 $\frac{3}{2}$  was observed, differing from the initially prescribed spin value of  $S = \frac{5}{2}$ . A series of static calculations were then performed to further probe this system and assess any potential instability of the manganese.

The results, shown in Figure 4.3, revealed a significant transition in the spin state. As the manganese atom moved out of the porphyrin plane, a spin transition occurred at around  $0.4 \,\text{Å}$ , with the spin-up states increasing and the spin-down states decreasing. This indicated a transition from an intermediate spin state (S=3) to a high-spin state (S=5).

An analysis of the d-orbital occupations, presented in the integrated DOS table 4.1, provided further evidence for this transition. The in-plane (low spin) configuration exhibited a total net spin of 3.1864 for the d-orbitals, while the out-of-plane (high spin) configuration displayed a substantially higher net spin of 4.4710. This is inline with the Muliken analysis that showed an oxidation state change form roughly Mn³ (low spin) to Mn² (high spin). From 4.1 it can be seen that these electrons are lost from the  $d_{yz}$  and  $d_{xy}$  orbitals. Notably, the  $d_{xy}$  orbital showed a significant shift in both its occupation and its energy, with its net spin increasing from 0.1683 to 0.8092 and its mean energy level shifting from -0.1678 eV to -0.7630 eV upon displacement out-of-plane. These energy values were taken by computing the mean or centroid of each of the orbitals spin density's.

This stabilisation of the  $d_{xy}$  orbital upon displacement resembled the mechanism observed for the perovskite  $Ca_{2-x}Mn_xTi_2O_6$  and the (NaY)MnMnTi<sub>4</sub>O<sub>12</sub> system, where the Mn<sup>2+</sup> displacement from the coplanar position was similarly driven by a lowering of the xy-orbital energy. However, a key difference was that the perovskite system maintained a constant Mn<sup>2+</sup> spin polarisation with a high-spin  $d^5$  configuration ( $S=\frac{5}{2}$ ) throughout the displacement, without undergoing the marked spin-state transition observed in the porphyrin system. Furthermore, the occupation of the xy-orbital did not change in the perovskite.

Figure 4.4 illustrates the changes in the d-orbitals as the Mn transitioned between in-plane (red) and out-of-plane (blue) configurations. A notable feature was the presence of negative spin density below the Fermi level in the in-plane configuration. Examination of Table 4.1 revealed that this spin density was associated with the  $d_{xz}$  orbital. According to Hund's rules, one would expect this orbital to align with the other d-orbitals and exhibit positive spin. This discrepancy may have arisen from an issue with the exchange–correlation treatment in DFT, which is further discussed later in this section. Unfortunately, it was not possible to probe the energetics of an in-plane  $S=\frac{5}{2}$  configuration because this static calculation failed to achieve self-consistency, and the electronic ground state was not found.

Due to the difficulties in modelling the high-spin state and the molecule's apparent preference for the lower spin  $(S=\frac{3}{2})$  configuration, it was difficult to draw firm conclusions regarding the spin transition and d-orbital energy redistribution, or whether it was indeed governed by a mechanism similar to that in (NaY)MnMnTi<sub>4</sub>O<sub>12</sub> and Ca<sub>2-x</sub>Mn<sub>x</sub>Ti<sub>2</sub>O<sub>6</sub>. Although the energetic redistributions of the d-orbitals appeared to support this mechanism directionally, it was also evident that, even after the transition to the  $S=\frac{5}{2}$  spin state, there remained a clear energetic favourability for a configuration closer to the plane of the porphyrin. However, because the transition occurred at displacements above 0.4 Å (where manganese was observed to move out-of-plane in the perovskite), it is possible that other effects, such as weaker bonding between the Mn and its coordination environment, began to dominate at higher displacements.

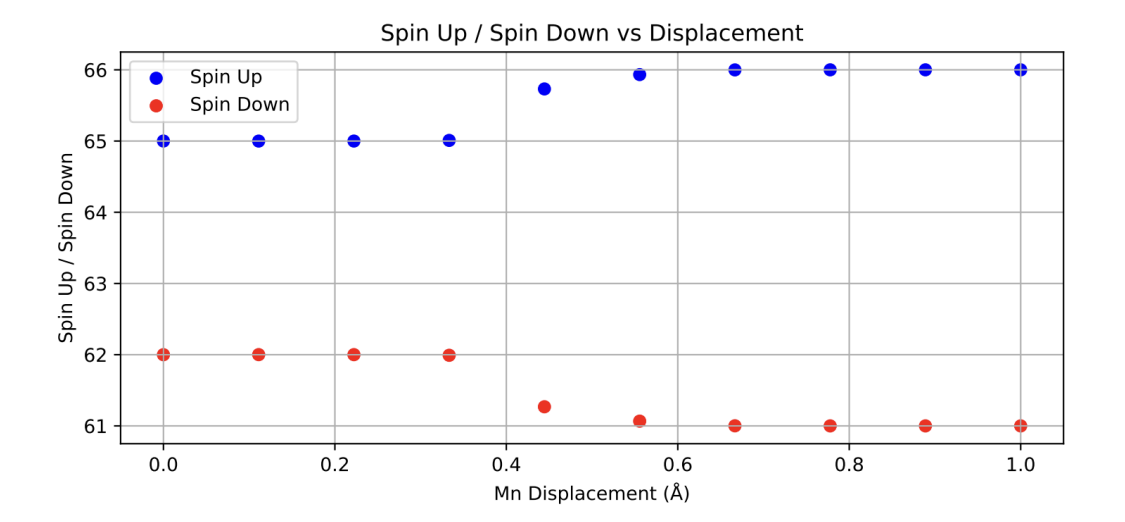


FIGURE 4.3: Spin polarization as a function of Mn displacement from the porphyrin plane. This is the total spin of the system although spin polarisation is entirely localised to Mn. As the Mn ion moves out of the N coordination plane, there is a transition from a low-spin Mn³ state to a high-spin Mn² state, demonstrated by the increase in spin-up (blue) and decrease in spin-down (red) electron populations.

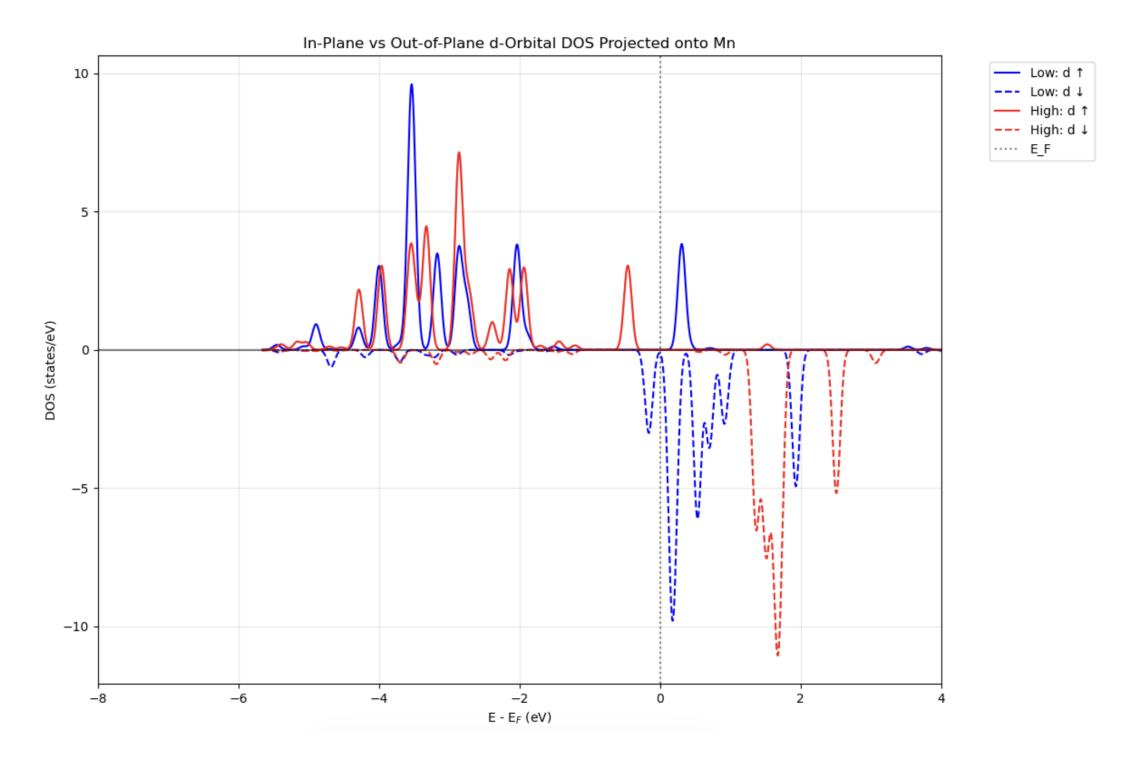


FIGURE 4.4: Projected density of states (PDOS) of d-orbitals for manganese in porphyrin systems, comparing in-plane (red) and out-of-plane (blue) configurations. The plot shows the distribution of electronic states relative to the Fermi level (E-Ef = 0, indicated by vertical dotted line). Positive values represent spin-up states while negative values represent spin-down states.

2*d Orbital	In-Plane (Low Spin)			Out-	of-Plane (High	n Spin)		
	Spin-up	Spin-down	Net ( <b>↑-</b> ↓)	Spin-up	Spin-down	Net ( <b>↑-</b> ↓)		
Integrated DOS over energy range [-5.66 eV, 0.00 eV]								
$\overline{d_{z^2}}$	0.8268	0.0250	0.8018	0.9683	0.0239	0.9444		
$d_{xz}$	0.9420	0.4692	0.4727	0.9538	0.0704	0.8833		
$d_{yz}$	0.8689	0.0171	0.8518	0.9637	0.0404	0.9233		
$d_{x^2-y^2}$	0.9610	0.0693	0.8917	0.9736	0.0629	0.9107		
$d_{xy}$	0.3142	0.1459	0.1683	0.9383	0.1291	0.8092		
d total	3.9129	0.7265	3.1864	4.7977	0.3267	4.4710		
Total	4.2287	0.8855	3.3431	5.2421	0.5630	4.6791		
Mean energ	Mean energy levels (centroids) [eV]							
$\overline{d_{z^2}}$		-0.8075			-0.3309			
$d_{xz}$		-0.3733			-0.4020			
$d_{yz}$		-0.4336			-0.5907			
$d_{x^2-y^2}$		-0.8552			-0.5840			
$d_{xy}$		-0.1678			-0.7630			

TABLE 4.1: Manganese Porphyrin In-Plane (Low Spin) and Out-of-Plane (High Spin) Electronic Structure Analysis.

## 4.1.3 Variations of Molecule and Packing Arrangements

When Kirner et al. reported unusual thermal parameters for the manganese atom perpendicular to the porphyrin plane in MnTPP, the measurements were made on a closely packed configuration with a separation of approximately 4Å [14].

Furthermore, a study on the close packing of MnP indicated that the ground-state electronic configuration might differ between isolated molecules and crystalline arrangements. In this investigation, it was observed that while isolated MnP molecules favoured a 4Eg ground state, the crystal structure of -phase MnP exhibited a 4A2g ground state. This difference was attributed to weak axial interactions with nitrogen atoms from adjacent molecules, whereby "two aza nitrogen atoms of each molecule lie exactly above or below the metal belonging to their nearest neighbours" at distances of approximately 3.2Å [35].

These observations motivated a systematic study, similar to that outlined previously for the MnP system. To investigate the influence of different packing arrangements as illustrated in 4.6 on manganese porphyrin systems, various intermolecular separations and configurations were explored.

Our computational results, as illustrated in 4.5, revealed that although different intermolecular separations did not fundamentally alter the spin transition observed upon manganese displacement from the porphyrin plane, they did influence the precise displacement at which this transition occurred. The spin transition from an intermediate-spin state (S=3) to a high-spin state (S=5) consistently appeared across all packing arrangements, occurring at displacements between 0.4 and 0.6Å. We concluded that this effect was evident in both MnTPP and the staircase structure, thereby highlighting the robustness of this phenomenon across different molecular environments.

This consistent behaviour across varying intermolecular separations provided

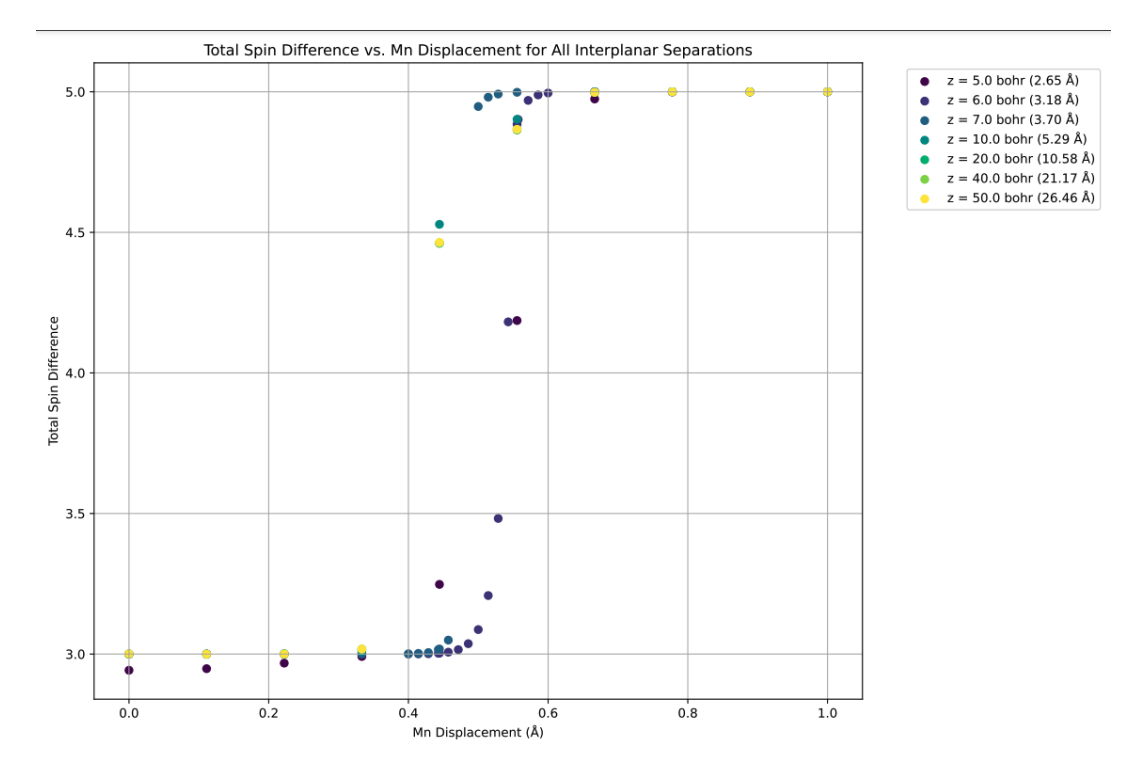


FIGURE 4.5: Total spin difference as a function of Mn displacement for various interplanar separations (labelled z) in stacked manganese porphyrin systems. The plot demonstrates that for all tested interplanar distances (ranging from 2.0 to 25.0 Å as indicated in the legend), a consistent spin transition occurs as the Mn atom is displaced from the porphyrin plane. The transition from a lower spin state (spin difference 3) to a higher spin state (spin difference 5) occurs primarily between 0.4-0.6 Å of displacement, regardless of the interplanar separation distance.

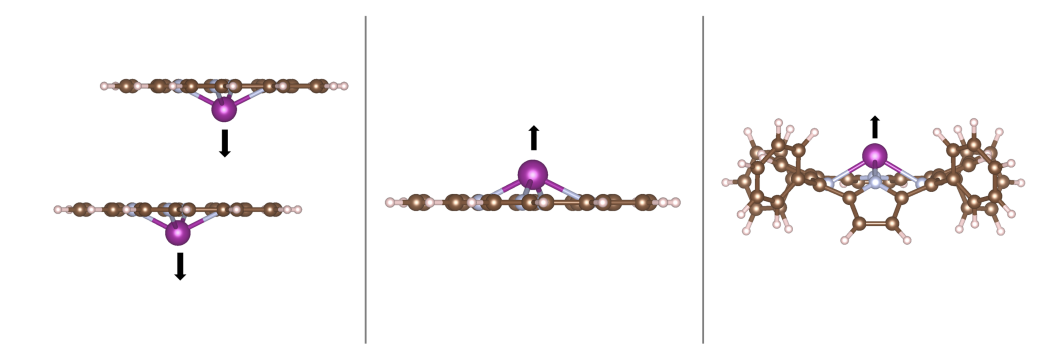


FIGURE 4.6: Structural models of different manganese porphyrin configurations used in displacement calculations. Left panel: Stacked manganese porphyrin with the Mn atom positioned above nitrogen atoms from adjacent molecules, with arrows indicating the displacement direction. Center panel: Regular manganese porphyrin in a vertical stacking arrangement, showing the Mn atom positioned above the porphyrin plane. Right panel: Manganese tetraphenylporphyrin (MnTPP).

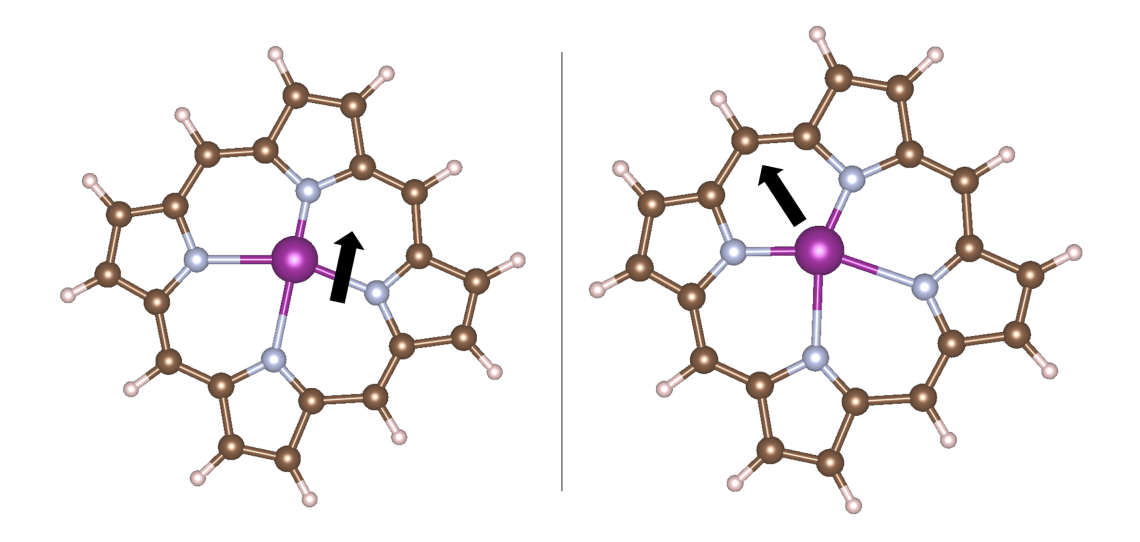


FIGURE 4.7: Manganese displaced along and adjacent to nitrogen atoms.

strong evidence that the fundamental mechanism driving the spin transition was intrinsic to the manganese–porphyrin coordination, rather than being primarily governed by intermolecular interactions. The slight shifts in the transition points observed with different packing distances indicated that, although these interactions could modulate the energetics of the transition, they did not alter its essential nature.

The staircase-like arrangement, in which manganese atoms resided atop the nitrogen atoms of adjacent molecules seen in Figure 4.6, was particularly noteworthy as it closely resembled the packing arrangement in -phase MnPc described by Liao et al. However, I saw the same spin transition as before and no energetic advantage to being out of plane. The MnTPP system also showed no energy advantage or differing spin configuration to what was obsever to MnP contradicting the experimental results observed by Kirner et al.

These findings weakly supported the initial hypothesis that the manganese porphyrin system exhibited behaviour analogous to the displacement mechanism observed in perovskite ferroelectrics, where A'-site cation displacements play a critical role in determining electronic properties. The persistence of the spin transition across different packing arrangements suggested that this mechanism was a fundamental feature of manganese coordination chemistry in porphyrinoid systems, thereby providing a simpler model system for studying the complex electronic transitions that occur in perovskite ferroelectrics.

### 4.1.4 Mn Displacement in Plane: Forced Symmetry Breaking

To investigate the role of symmetry breaking in manganese porphyrin systems, forced displacements of the manganese atom along various directions were examined. Two distinct displacement modes were considered: (1) a displacement along the axis directed toward a coordinating nitrogen atom, and (2) a diagonal displacement across the square-planar coordination environment. This approach permitted determination of whether the electronic transitions observed upon out-of-plane displacement were specifically dependent on the displacement direction. Similar to previous sections, a series of static calculations was conducted using the same previously relaxed structures. This procedure inherently produced elevated forces on the central

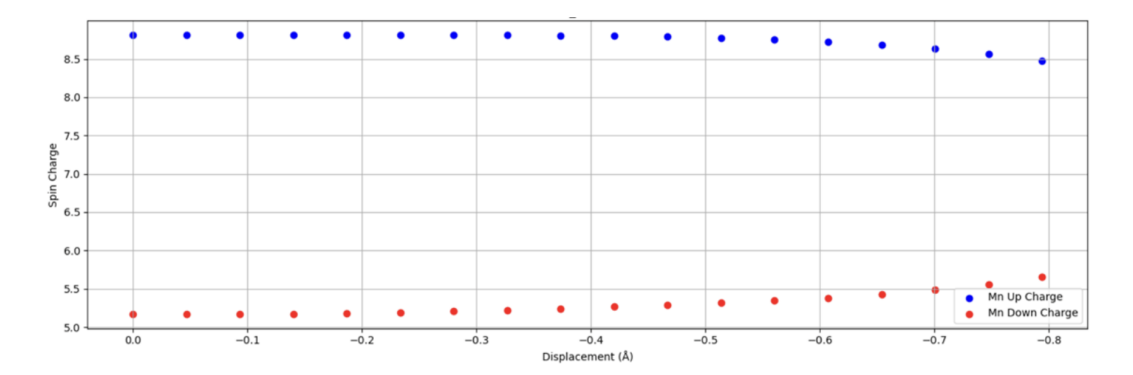


FIGURE 4.8: Spin charge distribution as a function of manganese displacement toward the porphyrin nitrogen atoms. The plot shows the Mn up charge (blue points) and Mn down charge (red points) as the manganese atom is displaced from 0 to -0.8 Å (negative values indicating movement toward the nitrogen plane).

Mn atom; consequently, the findings should be interpreted as indicative rather than definitive.

Computational results indicated a pronounced anisotropy in the electronic response to different displacement modes. Displacement of the manganese atom perpendicular to the porphyrin plane (along the c axis), as observed previously, triggered a distinct spin transition from an intermediate spin state (S=3) to a high spin state (S=5) at displacements between 0.4 and 0.6Å. In contrast, displacements toward a coordinating nitrogen atom (as seen in 4.8 diagonally across the square planar coordination environment did not yield any significant change in the spin state, with the spin value remaining approximately constant at S=3.5, irrespective of the displacement magnitude.

This directional dependence provided important insights into the underlying mechanism of the spin transition. The fact that spin changes occurred exclusively with out of plane displacements suggested that the electronic transition was not merely a function of variations in the Mn-N bond length but depended specifically on the symmetry of the displacement relative to the coordination environment. When manganese moved perpendicular to the porphyrin plane, it experienced a coordination environment in which the energy of the  $d_{xy}$  orbital was lowered relative to that of the  $d_{z^2}$  orbital, thereby facilitating electron redistribution that favoured the high spin state.

These findings paralleled the mechanism described for ferroelectricity in the perovskite  $Ca_{2-x}Mn_xTi_2O_6$ , in which the ordering of  $Mn^{2+}$  displacements along the c axis drives the ferroelectric transition. The observed directional preference for electronic transitions in the porphyrin system also depended on specific symmetry breaking rather than on a general distortion of the coordination sphere.

In summary, the results reinforced the conclusion that the manganese porphyrin system provided a suitable molecular model for investigating the displacement mechanism observed in perovskite ferroelectrics. In both cases, the specific direction of the metal displacement, rather than just its magnitude, played a critical role in determining the electronic properties of the material.

# 4.2 Issues Modelling High Spin Mn with DFT and Potential Solutions

#### 4.2.1 Ionic Relaxations

To explore whether the electronic transition observed in our static calculations corresponds to a stable structural feature, we performed ionic relaxation calculations using the same stacked manganese porphyrin systems. These calculations were designed to determine if the out-of-plane Mn configuration represents a local energy minimum in the potential energy surface. We employed comprehensive computational settings including a static run with SCF convergence tolerance of 1.0e-6, grid cutoff of 200 Ry for accurate charge density representation, Kerker preconditioning with a factor of 0.1 to aid convergence, and spin polarization enabled with appropriate settings for high-spin Mn. Despite the clear electronic transition observed in our static calculations, all relaxation attempts resulted in the Mn atom returning to the in-plane configuration, regardless of the initial displacement. This suggests that while the out-of-plane configuration shows interesting electronic properties, it does not represent a stable structural minimum in these porphyrin systems. We attempted to stabilize the out-of-plane configuration by constraining the spin polarization to a value of 5, corresponding to the high-spin state observed in our static calculations. However, these calculations failed to converge, indicating fundamental challenges in modelling this particular electronic state. Similarly, attempts to perform a static calculation with a fixed spin of 5 for the in-plane configuration were unsuccessful. These convergence difficulties suggest potential limitations in our DFT approach for modelling the high-spin d-orbital configuration in this system. Several factors may contribute to these challenges, including inadequate treatment of exchange-correlation effects for the partially filled d-orbitals, strong coupling between electronic and structural degrees of freedom, and multi-reference character of the electronic state that cannot be captured by single-reference DFT. These results highlight an interesting contrast between the electronic behaviour observed in our static calculations and the structural stability found in relaxation studies. While the spin transition and orbital reorganization with Mn displacement are clear electronic phenomena, they do not translate to stable structural features in the isolated porphyrin systems we studied.

#### 4.2.2 Potential Solutions

Future improvements to our approach could address the convergence challenges encountered when modelling the high spin state in planar manganese porphyrins. One promising strategy is to employ hybrid or meta GGA functionals that incorporate a larger fraction of exact exchange [36, 37]. Such functionals are expected to reduce self interaction and delocalisation errors present in the standard PBE functional, thereby enhancing the stability of the high spin configuration. An alternative approach would involve implementing a DFT+U correction, which may help to localise the manganese d electrons and increase the gap between the highest occupied and lowest unoccupied molecular orbitals, ultimately favouring the desired high spin state [38].

Additional refinement of the self consistent field procedure may also prove beneficial. Future work could explore the use of level shifting, increased damping and alternative initial density guesses, for example those based on broken symmetry or fragment methods, to guide the SCF towards the correct occupancy pattern [39]. It

may also be advantageous to relax the symmetry constraints slightly by allowing a minimal out of plane displacement of the manganese atom. Such a deliberate, small distortion would help to resolve any degeneracies in the electronic structure that currently lead to convergence difficulties. Once a stable high spin solution is achieved, it may then be possible to re enforce planarity and evaluate the persistence of the high spin state under strict geometric constraints.

These potential improvements represent promising future directions that could overcome the current limitations of our DFT approach in modelling the high spin configuration of manganese porphyrins.

29

#### 5. Conclusion

This report has presented a comprehensive computational investigation into two systems that, while differing in their structural complexities, exhibit a similar underlying mechanism related to metal centre displacement. In the columnar perovskite (NaY)MnMnTi4O12, our density functional theory (DFT) calculations reveal that ferroelectricity emerges from the interplay between a hybrid improper mechanism driven by partial A site cation ordering and a proper ferroelectric instability associated with the pseudo Jahn Teller activity of square planar Mn2+ ions. The energy landscape indicates that, in almost all examined cation ordering configurations, the Mn2+ ions predominantly adopt an out of plane displaced configuration. Notably, one particular initial ordering was observed in which the Mn ions remained close to the square planar sites. This unique case facilitated a direct energetic comparison, revealing that the system favours the out of plane (popped out) configuration by an energy difference of approximately 0.11 eV. Furthermore, the d orbital energetics observed in this NaY perovskite system share significant similarities with those reported in Ca2 x MnTi2O6; in both cases, the displacement of Mn drives a redistribution in d orbital energies, with a marked lowering of the d xy orbital. These observations suggest that a comparable underlying mechanism governs the ferroelectric instability in both perovskite systems.

In parallel, the investigation of organic manganese systems, comprising manganese porphyrins and phthalocyanines, demonstrated that when the Mn centre is driven out of its ligand plane, a pronounced reorganisation of the d orbitals occurs. Static DFT calculations show that this displacement is accompanied by a transition from an intermediate spin state (S=3) to a high spin state (S=5), with the d xy orbital exhibiting significant changes in both its occupation and mean energy level. Although the energetic preference for the high spin configuration in the organic systems is not as robust—in fact, the planar configuration appears energetically favourable—the observed spin transition and corresponding d orbital reorganisation share notable parallels with the behaviour seen in the Ca based perovskite system. This indicates that similar electronic interactions are at work, even though the organic systems do not exhibit a stable ferroelectric state.

An important consideration for future work is the potential to enhance the computational methodology. Although linear scaling in the CONQUEST code was not exploited in the current study, its implementation in future research could allow for the modelling of much larger cell sizes. This capability would facilitate the exploration of more intricate cation ordering patterns and enable systematic studies of domain formation and long range order in ferroelectric perovskites. Additionally, further refinements such as the adoption of hybrid or meta GGA functionals with a higher fraction of exact exchange, DFT U corrections, and improved self consistent field procedures (including level shifting and alternative initial density guesses) are anticipated to overcome the present limitations in converging high spin states for planar manganese porphyrins.

In summary, while the perovskite and organic systems investigated herein are not fundamentally identical, the comparative analysis provides important insights into how metal centre displacement drives electronic reorganisation in both material classes. The energy results, notably the energetic benefit associated with Mn displacement in the perovskite, and the similarities in d orbital energetics with the

5. Conclusion

Ca system, support the proposition that a similar mechanism may underlie the observed ferroelectric instabilities. This work establishes a foundation for further studies aimed at designing multifunctional materials in which controlled manipulation of cation ordering, metal displacement and spin state transitions can be harnessed to achieve targeted electronic and magnetic properties.

# **Bibliography**

- [1] J. Valasek, "Piezoelectric and Allied Phenomena in Rochelle Salt," in Proceedings of the American Physical Society, vol. XV, no. 6, p. 525, 1920.
- [2] F. Jona and G. Shirane, "Neutron diffraction study of orthorhombic BaTiO<sub>3</sub>," Physical Review, vol. 105, no. 3, pp. 856-860, 1957.
- [3] A. Aimi, D. Mori, K. Hiraki, T. Takahashi, Y. J. Shan, Y. Shirako, J. Zhou, and Y. Inaguma, "High-pressure synthesis of magnetic and ferroelectric CaMnTi<sub>2</sub>O<sub>6</sub>," Chemistry of Materials, vol. 26, no. 8, pp. 2601–2608, 2014.
- [4] R. E. Cohen, "Origin of ferroelectricity in perovskite oxides," Nature, vol. 358, no. 6382, pp. 136–138, Jul. 1992.
- [5] N. A. Benedek and C. J. Fennie, "Hybrid improper ferroelectricity: a mechanism for controllable polarization-magnetization coupling," Physical Review Letters, vol. 106, no. 10, p. 107204, 2011.
- [6] J. Cong, K. Zhai, Y. Chai, D. Shang, D. D. Khalyavin, R. D. Johnson, D. P. Kozlenko, S. E. Kichanov, A. M. Abakumov, A. A. Tsirlin, L. Dubrovinsky, X. Xu, Z. Sheng, S. V. Ovsyannikov, and Y. Sun, "Spin-induced multiferroicity in the binary perovskite manganite Mn<sub>2</sub>O<sub>3</sub>," Nature Communications, vol. 9, no. 2996, pp. 1–7, 2018.
- [7] H. A. Jahn and E. Teller, "Stability of polyatomic molecules in degenerate electronic states—I. Orbital degeneracy," Proceedings of the Royal Society of London. Series A, Mathematical and Physical Sciences, vol. 161, no. 905, pp. 220–235, 1937.
- [8] M. Manzi, G. Pica, M. De Bastiani, S. Kundu, G. Grancini, and M. I. Saidaminov, "Ferroelectricity in Hybrid Perovskites," Journal of Physical Chemistry Letters, vol. 14, pp. 3535–3552, 2023.
- [9] O. Auciello, J. F. Scott, and R. Ramesh, "The physics of ferroelectric memories," Physics Today, vol. 51, no. 7, pp. 22-27, 1998.
- [10] K. M. Rabe, C. H. Ahn, and J.-M. Triscone (Eds.), "Physics of Ferroelectrics: A Modern Perspective," Topics in Applied Physics, vol. 105, Springer-Verlag, 2007.
- [11] G. Gou, N. Charles, J. Shi, and J. M. Rondinelli, "A-site ordered double perovskite CaMnTi<sub>2</sub>O<sub>6</sub> as a multifunctional piezoelectric and ferroelectric-photovoltaic material," Inorganic Chemistry, vol. 56, no. 20, pp. 11854-11861, 2017.
- [12] N. A. Benedek and C. J. Fennie, "Why are there so few perovskite ferroelectrics?," The Journal of Physical Chemistry C, vol. 117, no. 26, pp. 13339–13349, 2013.
- [13] Z. Li, Y. Cho, X. Li, X. Li, A. Aimi, Y. Inaguma, J. A. Alonso, M. T. Fernandez-Diaz, J. Yan, M. C. Downer, G. Henkelman, J. B. Goodenough, and J. Zhou,

32 BIBLIOGRAPHY

"New Mechanism for Ferroelectricity in the Perovskite  $Ca_{2-x}Mn_xTi_2O_6$  Synthesized by Spark Plasma Sintering," Journal of the American Chemical Society, vol. 140, no. 6, pp. 2214-2220, 2018.

- [14] J. F. Kirner, C. A. Reed, and W. R. Scheidt, "Stereochemistry of manganese porphyrins. 2. The toluene solvate of  $\alpha$ ,  $\beta$ ,  $\gamma$ ,  $\delta$ -tetraphenylporphinatomanganese(II) at 20 and -175°C," Journal of the American Chemical Society, 99(4), pp. 1093–1101, 1977.
- [15] H. Jiang, P. Hu, J. Ye, R. Ganguly, Y. Li, Y. Long, D. Fichou, W. Hu, and C. Kloc, "Hole mobility modulation in single-crystal metal phthalocyanines by changing the metal– $\pi/\pi$ – $\pi$  interactions," Angewandte Chemie International Edition, 57(32), pp. 10112–10117, 2018.
- [16] P. Hohenberg and W. Kohn, "Inhomogeneous Electron Gas," *Physical Review*, vol. 136, no. 3B, pp. B864–B871, 1964.
- [17] W. Kohn and L. J. Sham, "Self-Consistent Equations Including Exchange and Correlation Effects," *Physical Review*, vol. 140, no. 4A, pp. A1133–A1138, 1965.
- [18] R. M. Martin, *Electronic Structure: Basic Theory and Practical Methods*, Cambridge University Press, 2004.
- [19] D. M. Ceperley and B. J. Alder, "Ground State of the Electron Gas by a Stochastic Method," *Physical Review Letters*, vol. 45, no. 7, pp. 566–569, 1980.
- [20] J. P. Perdew and Y. Wang, "Accurate and simple analytic representation of the electron-gas correlation energy," *Physical Review B*, vol. 45, no. 23, pp. 13244–13249, 1992.
- [21] R. G. Parr and W. Yang, Density-Functional Theory of Atoms and Molecules, Oxford University Press, 1989.
- [22] D. R. Bowler and T. Miyazaki, "O(N) methods in electronic structure calculations," *Reports on Progress in Physics*, vol. 75, no. 3, p. 036503, 2012.
- [23] D. R. Bowler, T. Miyazaki, and M. J. Gillan, "Recent progress in linear scaling ab initio electronic structure techniques," *Journal of Physics: Condensed Matter*, vol. 14, no. 11, pp. 2781–2798, 2002.
- [24] R. McWeeny, "Some Recent Advances in Density Matrix Theory," *Reviews of Modern Physics*, vol. 32, no. 2, pp. 335–369, 1960.
- [25] P. Pulay, "Convergence acceleration of iterative sequences. The case of SCF iteration," *Chemical Physics Letters*, vol. 73, pp. 393–398, 1980.
- [26] G. Kerker, "Electronic structure of LiN," *Physical Review B*, vol. 23, no. 12, pp. 6312–6318, 1981.
- [27] A. Nakata, J. S. Baker, S. Y. Mujahed, J. T. L. Poulton, S. Arapan, J. Lin, Z. Raza, S. Yadav, L. Truflandier, T. Miyazaki, and D. R. Bowler, "Large scale and linear scaling DFT with the CONQUEST code," *Journal of Chemical Physics*, vol. 152, no. 16, p. 164112, 2020.
- [28] D. R. Bowler and T. Miyazaki, "Highly accurate local basis sets for large-scale DFT calculations in CONQUEST," *Journal of Physics: Condensed Matter*, vol. 32, no. 47, p. 475901, 2020.

BIBLIOGRAPHY 33

[29] A. Aimi, D. Mori, K. Hiraki, T. Takahashi, Y. J. Shan, Y. Shirako, J. Zhou, and Y. Inaguma, "High-pressure synthesis of magnetic and ferroelectric CaMnTi<sub>2</sub>O<sub>6</sub>," *Chemistry of Materials*, vol. 26, no. 8, pp. 2601–2608, 2014.

- [30] F. Jona and G. Shirane, Ferroelectric Crystals (Pergamon Press, Oxford, 1962).
- [31] V. M. Goldschmidt, Naturwissenschaften 14, 477 (1926).
- [32] N. A. Benedek and C. J. Fennie, J. Phys. Chem. C 117, 13339 (2013).
- [33] R. Scatena et al., Angew. Chem. Int. Ed. 2023, e202305994 (2023).
- [34] Z. Li et al., J. Am. Chem. Soc. 140, 2214 (2018).
- [35] M.-S. Liao, J. D. Watts, and M.-J. Huang, "DFT Study of Unligated and Ligated Manganese II Porphyrins and Phthalocyanines," *Inorganic Chemistry*, vol. 44, no. 6, pp. 1941–1949, 2005.
- [36] M. Kaupp, "Recent advances in computational studies of ferroelectricity in transition metal compounds," *Molecules*, vol. 28, no. 12, pp. 3487–3500, 2023.
- [37] K. Pierloot, "The electronic structure of transition metal compounds: contributions from multireference wavefunction theory," *The Journal of Physical Chemistry A*, vol. 112, pp. 11824–11838, 2008.
- [38] K. Leung, A. J. Cohen and R. Streitwieser, "The DFT+U approach applied to transition-metal porphyrins," *Inorganic Chemistry*, vol. 45, no. 13, pp. 5142–5150, 2006.
- [39] P. Morgante and R. Peverati, "Challenges in converging high spin states in transition metal complexes using density functional theory," *Molecules*, vol. 28, no. 15, pp. 4876–4890, 2023.
- [40] I. D. Brown and R. D. Shannon, "Empirical bond-strength-bond-length curves for oxides," Acta Crystallographica Section A: Crystal Physics, Diffraction, Theoretical and General Crystallography, vol. 29, no. 3, pp. 266–282, 1973.